Aerosol and Air Quality Research

ORIGINAL RESEARCH
https://doi.org/10.4209/aaqr.220311

Analysis of Surface Level $PM_{2.5}$ Measured by Low-Cost Sensor and Satellite-Based Column Aerosol Optical Depth (AOD) over Kathmandu

Jeevan Regmi[1,2], Khem N. Poudyal[3], Amod Pokhrel[4], Nabin Malakar[5], Madhu Gyawali[6], Lekhendra Tripathee[7], Mukesh Rai[7], Srikanthan Ramachandran[8], Katrina Wilson[9], Rudra Aryal[9*]

[1] Prithvi Narayan Campus, Tribhuvan University (TU), Pokhara, Nepal
[2] Central Department of Physics, Tribhuvan University, Kirtipur, Nepal
[3] Department of Applied Sciences, IOE Pulchowk Campus, Tribhuvan University, Lalitpur, Nepal
[4] University of California Berkeley, California, USA
[5] Worcester State University, Massachusetts, USA
[6] Department of Physics, San Jacinto College, South Campus, Houston, TX 77089, USA
[7] State Key Laboratory of Cryospheric Science, Northwest Institute of Eco-Environment and Resources, Chinese Academy of Sciences, Lanzhou 730000, China
[8] Physical Research Laboratory, Ahmedabad, India
[9] Franklin Pierce University, Rindge, NH, USA

ABSTRACT

A low-cost PurpleAir PA-II sensor was installed, in 2020 at the Institute of Engineering (IOE) Pulchowk Campus, TU located in Kathmandu valley, Nepal, to measure particulate matter with an aerodynamic diameter equal to or smaller than 2.5 μm ($PM_{2.5}$). The observation shows that hourly averaged $PM_{2.5}$ fluctuates bimodally in four seasons (Winter: December, January, and February; Spring: March–May; Summer: June–September; and Autumn: October–November), with the highest levels occurring during morning and evening rush hours. PurpleAir records $PM_{2.5}$ with a maximum average of 101 ± 26.31 μg m^{-3}, in winter, 55.58 ± 11.42 μg m^{-3}, in spring, 45.46 ± 12.16 μg m^{-3}, in autumn, and a minimum of 22.78 ± 3.23 μg m^{-3}, in the summer. Due to rain and diffusion in the vertical atmosphere, $PM_{2.5}$ levels are lowest during the summer. The ± number for each season represents the standard deviation from the hourly average. AOD_{550nm} data collected by MODIS (Moderate Resolution Imaging Spectroradiometer) onboard two NASA satellites, Terra and Aqua, are compared with simultaneously observed $PM_{2.5}$. With humidity correction factor f(RH), R^2 increases from 0.413 to 0.608 (in winter), 0.426 to 0.508 (in spring), and 0.083 to 0.293 (in autumn). The summer AOD data and $PM_{2.5}$ are not compared due to a lack of AOD observations. By comparing the column-integrated aerosol data with the surface-level aerosol concentration, this study illustrates the relevance of atmospheric parameters while investigating the reliability of PurpleAir measurements. A cluster analysis of five-day back trajectories of air masses arriving at different altitudes in different seasons indicates that long-range transport of air pollution contributes to MODIS's column integrated AOD by adding aerosol population.

Keywords: Aerosol optical depth, MODIS, $PM_{2.5}$, PurpleAir, Transboundary aerosols

OPEN ACCESS

Received: September 20, 2022
Revised: November 28, 2022
Accepted: December 15, 2022

* **Corresponding Author:**
aryalr@franklinpierce.edu

Publisher:
Taiwan Association for Aerosol Research
ISSN: 1680-8584 print
ISSN: 2071-1409 online

1 INTRODUCTION

The study of atmospheric aerosols, particulate matter, is important since they influence Earth's radiation budget by scattering and absorbing incoming solar radiation and altering cloud microphysical properties (Haywood and Boucher, 2000; Ramanathan *et al.*, 2001). Their ability to affect Earth's radiation budget and their effects on health, air quality, and clouds are strongly

related to their size (Dusek *et al.*, 2006; Ruzer and Harley, 2005). A $PM_{2.5}$ particle has an aerodynamic diameter of less than 2.5 micrometers. Particulates of this size can be either natural or anthropogenic, and their composition varies according to their sources (Devi *et al.*, 2020). Human-produced particles are generally smaller in size, while naturally produced particles are larger. $PM_{2.5}$ is also one of the most common pollutants contributing to global health burdens (Lim et al., 2012). According to Shiraiwa *et al.* (2017), these particles penetrate deeply into the lungs of humans and cause adverse health effects depending on their chemical composition. Statistical analysis shows a strong correlation between hospitalizations, and deaths and exposure to high $PM_{2.5}$ concentrations (Di *et al.*, 2017; Schwartz *et al.*, 1996; Klemm and Mason, 2000). As a result, a comprehensive measurement and analysis of particle concentration in the atmosphere are essential for protecting local health and studying atmospheric conditions.

Several studies highlight the importance of low-cost air quality monitoring instruments, such as PurpleAir Monitors, for determining both spatial and temporal air quality, since traditional real-time air quality monitors lack this capability due to their high installation and maintenance costs (Kumar *et al.*, 2018; Munir *et al.*, 2019). Because of their availability, size, and price, PurpleAir monitors are being widely used in almost every continent to measure PM concentrations on surfaces, as well as for assessing air pollution (Ouimette *et al.*, 2022).

These monitors work on the light scattering principle in which a fan draws air particles into the chamber and passes along the laser path. The sensor's photodiode detector converts scattered light into voltage pulses from light. These pulses use to count the number of particles of sizes 0.3, 0.5, 1, 2.5, 5, and 10 μm and determine mass concentrations of $PM_{1.0}$, $PM_{2.5}$, and PM_{10} by using an algorithm for PM concentration (Ardon-Dryer *et al.*, 2020; Sayahi *et al.*, 2019); https://www2.purpleair.com/community/faq). In a variety of environmental conditions, PurpleAir monitors were evaluated for measuring atmospheric particle concentrations (Morawska *et al.*, 2018; Stavroulas *et al.*, 2020; Zhang *et al.*, 2009). Ardon-Dryer *et al.* (2020) showed that PurpleAir $PM_{2.5}$ data significantly correlated with $PM_{2.5}$ measured by AQMS (Air Quality Monitoring Stations) operated by the Environmental Protection Agency. This study will also aid in investigating the low-cost monitors for measuring air pollution by comparing them with other reliable reference data, such as satellite-based aerosol optical properties. The simultaneous measurements of aerosols at ground level and those based on remote sensing provide reliable information about air pollutant loading over the observation site (Baral and Thapa, 2021; Segura *et al.*, 2017). Comparison of surface and atmospheric level aerosol data can also be used as a statistical basis to extrapolate regional aerosol data (Aryal *et al.*, 2014; Moody *et al.*, 2014).

In atmospheric column observations, satellites provide long-term data and global coverage, providing insights into regional air quality and climate variations through the precise timing and spatial resolution of $PM_{2.5}$ concentrations (Karagulian *et al.*, 2015; Schwarze *et al.*, 2006; Zhong *et al.*, 2015). Satellites, however, view the entire atmosphere column, which makes it difficult to distinguish surface-level particle concentrations. Therefore, ground-based measurements and comparisons with satellite-based aerosol data can lower the uncertainty associated with local and external aerosols, and meteorological parameters (Kumar *et al.*, 2007).

The use of low-cost sensors in surface measurements can alleviate the limitations of human resources and can enable setting up multiple ground-based measurement stations easier, regardless of a lack of funding and/or technical expertise. A correlative analysis based on satellite-based aerosol optical depth (AOD) data and ground-level particle concentration can be conducted to evaluate the proposed method for estimating $PM_{2.5}$ in areas that lack ground-level observations (van Donkelaar *et al.*, 2015).

Several studies have examined the air quality and aerosol loading trend over the Kathmandu Valley (Aryal *et al.*, 2009; Islam *et al.*, 2020; Mahapatra *et al.*, 2019). MODIS-equipped Earth observation satellites Terra and Aqua pass over the Kathmandu valley every morning and afternoon (at about 10:30 am and 1:00 pm local time, respectively), and MODIS' AOD data (3 km × 3 km) can be used to compare with surface level $PM_{2.5}$ (Ramachandran and Kedia, 2013).

This paper will present and analyze the hourly variability of $PM_{2.5}$ observed by PurpleAir monitor at the Pulchowk Engineering Campus (TU), located about a hundred meters from the bus station, for each season and compare surface-level particle concentrations with satellite-based AODs using relative humidity correction factor. Relative humidity influences aerosol particle growth and refractive index, affecting aerosol mass concentration (Altaratz *et al.*, 2013; Hagan and Kroll,

2020; Malm *et al.*, 2000). Kathmandu valley's bowl-shaped structure and surrounding mountains make it a unique case study for investigating air pollution (Kitada and Regmi, 2003; Panday and Prinn, 2009; Shakya *et al.*, 2017; Shrestha *et al.*, 2017). This paper also presents the local and regional aspects of long-range air pollution transport over Kathmandu Valley using cluster analysis of back trajectory air masses arriving over the observation site.

2 MATERIALS AND METHODS

2.1 Site Description

A PurpleAir sensor was deployed in the Kathmandu valley (Pulchowk Engineering Campus, IOE, Lalitpur, Lat. 27.68°N, Long. 85.31°E, and Alt. 1350 m Fig. 1) to measure real-time $PM_{2.5}$ concentration data. The city of Kathmandu is Nepal's largest metropolitan area and is highly polluted. Nepal is surrounded by the Indo-Gangetic Plain in the south and the large Himalayas in the north (Shakya *et al.*, 2017; Regmi *et al.*, 2020). High mountains surround the Kathmandu valley, ranging from 2000 meters to 2800 meters, and the valley is shaped like a bowl, trapping pollution.

This city is experiencing rapid urbanization and population growth. The region is characterized by haphazard construction, unmanaged industries, brick and kiln production, and solid waste and biomass burning. Kathmandu also experiences significant amount of transboundary air pollution (Kitada and Regmi, 2003). Transported dust aerosols impact the cloud microphysical properties significantly. As a result of biomass burning and dust storms in the Indo-Gangetic Plain region, and long-range transportation, aerosols accumulate over Nepal, which, when combined with local pollution sources, contributes to high levels of pollution (Adhikari and Mejia, 2022; Becker *et al.*, 2021; Das *et al.*, 2021; Jethva *et al.*, 2019; Regmi *et al.*, 2020).

2.2 PurpleAir, Sampling Methods and MODIS AOD

PurpleAir's website (https://www2.purpleair.com/) provides real-time $PM_{2.5}$ (in $\mu g\ m^{-3}$) data. Microprocessor-based circuits are used to calculate equivalent particle diameters and the number of particles with different diameters per unit volume (Ouimette *et al.*, 2022; Yong, 2016). The processing algorithms for the Plan-tower PMS5003 sensors (PA-PMS) used in the PurpleAir (PA) monitor configuration are provided in He *et al.* (2020). The remainder of this paper uses the

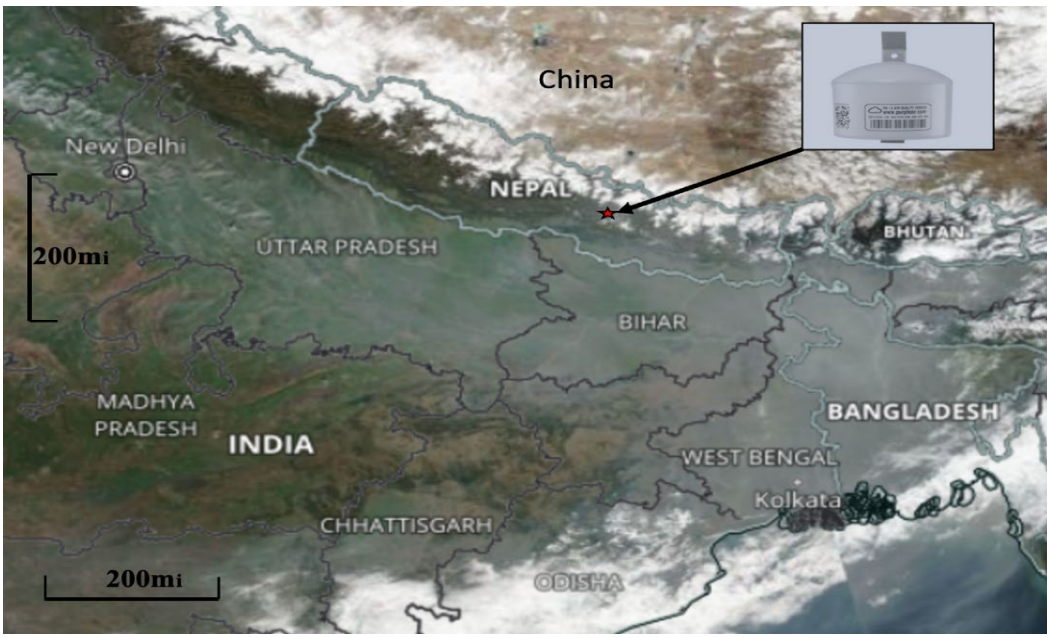

Fig. 1. As seen in the MODIS image (taken by NASA's Terra satellite on February 9, 2020), there is a noticeable accumulation of haze on the foothills of the Himalayan range. The top right corner of the figure shows a PurpleAir monitor located at Kathmandu Valley.

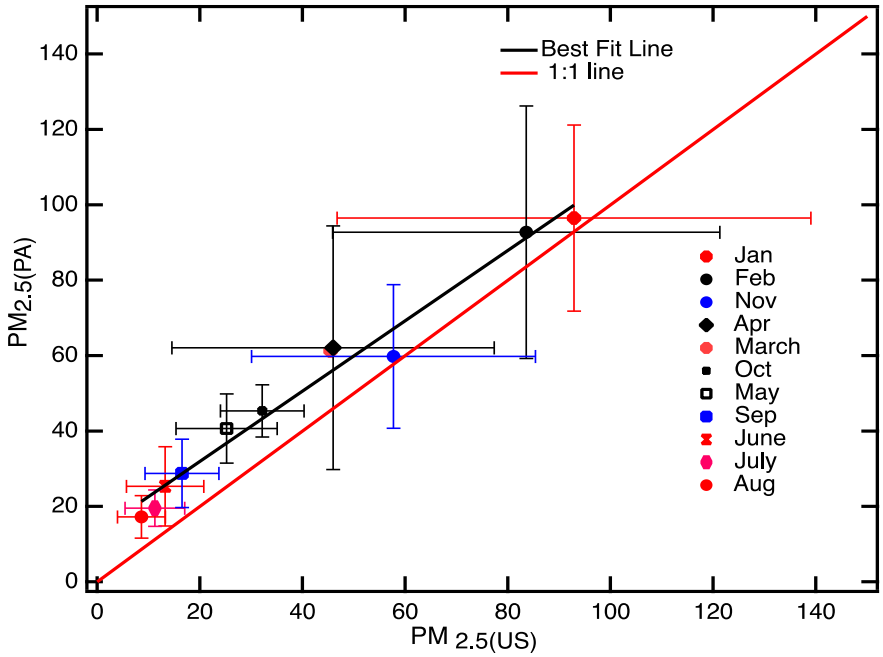

Fig. 2. The scatter plot shows the monthly averages for $PM_{2.5(PA)}$ and $PM_{2.5(US)}$ in unit of μg m^{-3}. Based on the legend in the figure, the symbols are ordered from higher to lower $PM_{2.5}$ for the different months. December month is discarded for comparison due to a lack of data availability.

symbol $PM_{2.5(PA)}$ for $PM_{2.5}$ observed by a PurpleAir monitor. Additionally, we compare $PM_{2.5(PA)}$ data with $PM_{2.5(US)}$ data to indicate the reliability of PurpleAir. $PM_{2.5(US)}$ is monitored by the Ambient Air Quality Monitoring Station (Beta Attenuation Monitor, BAM) at the Phora Durbar Recreation Center, 3 km from the PurpleAir monitoring site and supported by the United States Embassy (Edwards *et al.*, 2021). The BAM 1022 measures and records airborne PM concentrations in μg m^{-3} at local temperatures and atmospheric pressures by utilizing beta-ray attenuation (Magi *et al.*, 2020). The manufacturer's website provides a complete description of the BAM 1022's operation (https://metone.com/air-quality-particulate-measurement/regulatory/bam-1022/).

A significant correlation exists between $PM_{2.5(PA)}$ and $PM_{2.5(US)}$ data sets with a coefficient of determination (R^2) of 0.98. The best fit line equation is $PM_{2.5(PA)}$ = 0.93(± 0.04) $PM_{2.5(US)}$ + 13.23 (± 2.40) as shown in Fig. 2.

However, the two sets are not validated individually against other nearby reference optical devices. In Fig. 2, the scatter plot shows that PurpleAir data $PM_{2.5(PA)}$ near the bus station is slightly above the 1:1 line compared to $PM_{2.5(US)}$ at Phora Durbar and shows that $PM_{2.5(PA)}$ provides usable data representing the atmosphere of Kathmandu valley.

In this study, $PM_{2.5(PA)}$ is compared with NASA's MODIS column integrated Aerosol Optical Depth (AOD at 550 nm) product, which is corrected for relative humidity. The rest of this paper uses AOD_{550nm} to represent AOD retrieved from Satellite data. AOD_{550nm} aerosol products collected from MODIS Aqua and Terra at 3 km × 3 km is analyzed in this study. The 3 km × 3 km algorithm differs from the 10 km × 10 km algorithm simply in the way reflectance pixels are ingested, organized, and selected (Levy *et al.*, 2013). PurpleAir provides optical data matching the products of aerosol optical devices such as cell reciprocal and TSI 3563 integrating nephelometers, according to Calvello *et al.* (2008) and Ouimette *et al.* (2022).

2.4 Model Description

The relationship between PM and AOD is illustrated by a simplified linear equation with a relative humidity correction factor. To express a statistical model, we have written the particle concentration (PM) in general, observed at the ground level with the dry sample, which can be expressed quantitatively (Xu and Zhang, 2020) as

$$PM = \frac{4}{3}\pi\rho\int_0^\infty r^3 n_{dry}(r)dr \quad (1)$$

$n_{dry}(r)$ denotes the number of particles per unit volume in atmospheric space per unit particle radius and ρ is the aerosol particle density. Based on the hypothesis of spherical particles, the columnar AOD can be calculated using the Mie scattering theory with the equation (Calvello *et al.*, 2008), and can be written as,

$$AOD = \int_0^\infty dh \int_0^\infty \pi r^2 Q_{ext,amb}(r) n_{amb}(r,h)dr \quad (2)$$

where r is the radius of the assumed spherical particles, Q_{ext} is the extinction efficiency factor defined by van de Hulst (1981), and n_{amb} (r, h) represents the aerosol size distribution giving a concentration of particles per unit volume per particle radius at height h, which is factorized in two parts based on height.

$$(n_{amb}(r,h)) = n_{amb}(r)n(h) = n_0\, n_{amb}(r)\exp(-h/H) \quad (3)$$

where n_0 is the particle concentration at the surface level and H is the aerosol scale height, then the equation for AOD can be expressed as given by Calvello *et al.* (2008).

$$AOD = n_0 H\int_0^\infty \pi r^2 Q_{ext,amb}(r) n(r)dr \quad (4)$$

Several models explain the relationship between f(RH) and Relative humidity (RH) (Brock *et al.*, 2016, 2021; Chen *et al.*, 2016; Kasten, 1969; Kotchenruther and Hobbs, 1998; Zheng *et al.*, 2017). This work utilizes the f(RH) expression (Brock *et al.*, 2021; Zheng *et al.*, 2017) to examine aerosol light extinction induced by hygroscopic growth.

$$f(RH) = \frac{AOD}{AOD_{dry}} = \left(1 + \frac{RH}{100 - RH}\right) \quad (5)$$

where AOD_{dry} represents the aerosol optical depth with dehydration adjustment. Then the expression for AOD in terms of the dry condition can be expressed as,

$$AOD = n_0 H f(RH)\int_0^\infty \pi r^2 Q_{ext,dry}(r) n(r)dr \quad (6)$$

To investigate the AOD vs. PM relation, the size distribution and extinction efficiency $<Q_{ext}>$ and effective aerosol radius r_{eff} are expressed (Xu and Zhang, 2020) as,

$$<Q_{ext}> = \frac{\int_0^\infty Q_{ext}(r)n(r)r^2dr}{\int_0^\infty n(r)r^2dr} \quad (7)$$

And, the effective radius of aerosol particles is given as,

$$r_{eff} = \frac{\int_0^\infty n(r) r^3 dr}{\int_0^\infty n(r) r^2 dr} \quad (8)$$

Based on the above Eqs. (2), (4), (7), and (8) a relation between AOD/f(RH) and PM can be obtained as

$$AOD = \frac{3}{4} n_0 . H . f(RH) . PM \frac{< Q_{ext,dry}(r) >}{\rho r_{eff}} \quad (9)$$

Thus Eq. (9) provides, assuming H as a constant for all data for this study, f(RH) as the correcting factor to study the correlation between AOD/(f(RH)) vs. PM.

2.4 Statistical Analysis

AOD_{550nm} obtained from two satellite measurements, Aqua and Terra, is compared with the hourly averaged PurpleAir data $PM_{2.5(PA)}$. For comparison with ground based $PM_{2.5(PA)}$, the AOD_{550nm} are corrected by dividing with f(RH), where RH is ambient relative humidity. At different humidity levels, aerosol particles with different chemical compositions but the same mass concentration exhibit different aerosol optical properties (Jin *et al.*, 2022). Accordingly, this correlation study investigates the correlation between aerosol extinction and mass concentration using relative humidity correction factor, f(RH).

MOD04 and MYD04_3K data (MOD04 for Terra, MYD04 for Aqua), 3 km × 3 km AOD_{550nm} data were extracted and correlated with a temporal variation of $PM_{2.5(PA)}$ from PurpleAir sensors at ground level. AOD_{550nm} measurements from two satellites, Aqua and Terra, were observed simultaneously with $PM_{2.5(PA)}$ measurements. We performed the graphical analysis using the Levenberg-Marquardt least orthogonal distance method implemented in IGOR (https://www.wavemetrics.com/). The data were then analyzed using linear regression analysis, and a coefficient of determination (R^2) was obtained. A two-tailed P statistic and a coefficient of correlation coefficient (R) was calculated to determine the significance of the correlation. Data with confidence levels (based on P values) < 95% were disregarded for statistical significance.

2.5 Cluster Analysis

The aerosol particle trajectories arriving at Kathmandu at 500 m, 1000 m, and 1500 m asl were analyzed using cluster analysis to understand the origin of aerosol particles over Kathmandu Valley's vertical column. For each season, seasonal clusters were generated by analyzing five days of air mass trajectories starting at 500 m, 1000 m, and 1500 m asl over Kathmandu (Lat. 27.68°N, Long. 85.31°E) at 0:00, 6:00, 12:00, and 18:00 UTC each day. In this study, the cluster calculations were conducted using the free software Traj-stat (Regmi *et al.*, 2020; Wang, 2014).

3 RESULTS AND DISCUSSION

3.1 The Hourly Variation of the Seasonally Averaged $PM_{2.5}$

Fig. 3 shows hourly variations of $PM_{2.5(PA)}$ concentrations (in μg m^{-3}) for each season in 2020. The average maximum $PM_{2.5(PA)}$ is observed to be 101 ± 26.31 μg m^{-3} in the winter season, while the minimum is seen in summer (22.78 ± 3.23 μg m^{-3}). Similarly, the average concentration of 55.58 ± 11.42 μg m^{-3} is observed in the spring and 45.46 ± 12.16 μg m^{-3} in the autumn. The ± 1 σ standard deviation obtained from hourly averaged measurements for each season are given adjacent to the seasonal mean values. Kathmandu is a bowl-shaped urban basin in Nepal, and during winter, the planetary boundary layer is thinner due to the dense, cooler air near the surface. A layer of cooler air sits beneath the warm air above, forming a kind of lid in the atmosphere referred to as winter inversion. Only within this layer does vertical air mixing occur, so pollutants

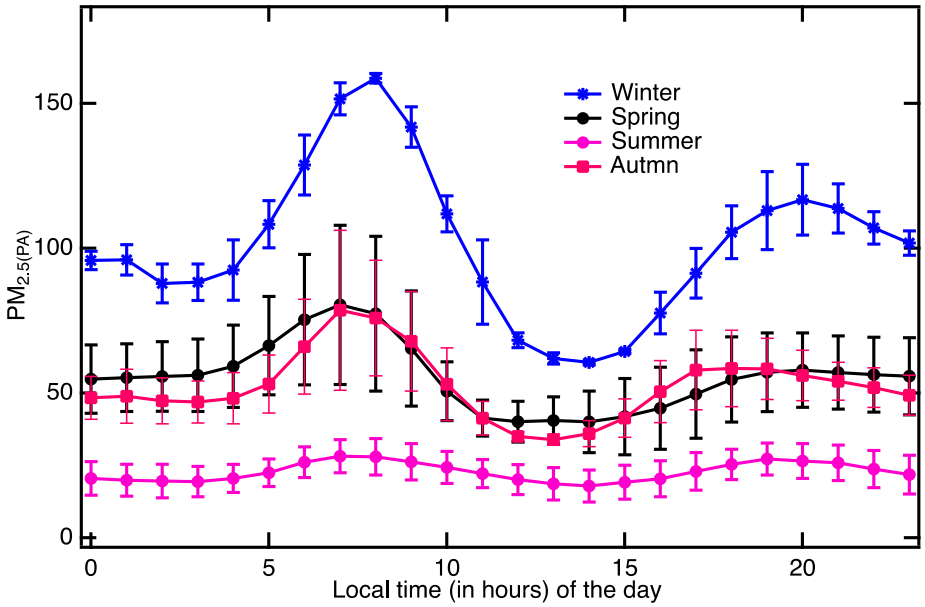

Fig. 3. Hourly averaged (at local time) averaged particle concentration ($PM_{2.5(PA)}$) in μg m^{-3} for each season by using the corresponding months' data for each season.

cannot disperse in the atmosphere. Kathmandu relies mainly on wood for heating in winter, and wood burning contributes significantly to air pollution. Kotchenruther (2020) found elevated levels of $PM_{2.5}$ during the winter in the Northwest U.S. According to the study, residential wood combustion, motor vehicle emissions, gaseous NO_x emissions, and particulate sulfate emissions are the primary sources of $PM_{2.5}$ during winter.

For all seasons, particle mass concentrations are bimodal, significantly higher in the mornings (around 8:00 am) and evenings (around 7:00 pm). Fig. 3 shows the seasonal variations of hourly averaged $PM_{2.5(PA)}$, which are bimodal in all seasons. The amplitude and width of $PM_{2.5(PA)}$ is maximum during the winter seasons, and the patterns are similar during spring, summer, and autumn. No significant variation in hourly averaged $PM_{2.5(PA)}$ is seen during summer. A signature of local activity can be seen in $PM_{2.5(PA)}$, such as during the household cooking and traffic emissions time. Many studies have shown that household and commercial cooking significantly contribute to $PM_{2.5}$ pollution in urban areas (Balasubramanian *et al.*, 2021; Pervez *et al.*, 2019; Robinson *et al.*, 2018). Earlier studies have also shown that traffic and cooking contribute to air pollution in Kathmandu valley during rush hours (morning and evening) and off hours in the afternoon (Islam *et al.*, 2020).

$PM_{2.5(PA)}$ increases gradually during rush hours in traffic. On a global scale, cooking and heating fuels contribute 20–55% to anthropogenic particle emissions (Balasubramanian *et al.*, 2021; Pervez *et al.*, 2019). The study concludes that domestic cooking and traffic are significant anthropogenic factors affecting the Kathmandu valley's surface-level $PM_{2.5(PA)}$ concentrations. Previously, it has been shown that traffic contributes significantly to air pollution in different urban areas, with coarse particles originating from non-exhaust sources like road abrasion, brake wear, and tire wear, while fine particles are emitted directly from fuel combustion (Kumar and Goel, 2016; Pant and Harrison, 2013). Low temperatures can lead to the formation of secondary aerosols during the winter months (Duan *et al.*, 2020; Mues *et al.*, 2018). Previous studies have shown the importance of secondary organic aerosols (SOA) in contributing to $PM_{2.5}$ (Bui *et al.*, 2022; Mancilla *et al.*, 2015).

Fig. 3 also shows that the average particle concentration at hourly averaged $PM_{2.5(PA)}$ decreases from winter to summer, then increases again in autumn as the seasons change. A rise in temperature in the summer causes surface-level particles to diffuse rapidly in the vertical atmosphere, resulting in lower surface concentrations. PurpleAir record shows an average temperature of 17.77 ± 4.00°C in winter, 24.08 ± 2.65°C in summer, and 28.96 ± 1.65°C in autumn. The summer also brings significant amounts of rain, which helps removal of aerosol particles from the atmosphere (Becker *et al.*, 2021). June to September are rainy monsoon months in Kathmandu, which can

significantly reduce air pollution. Thus, the monsoon rain also plays a crucial role in reducing the surface level air pollution in Kathmandu in the summer months from June to September. The COVID lockdown period from March to July also significantly reduced traffic flow, which might have affected particle concentrations in the atmosphere (Baral and Thapa, 2021).

3.2 Comparison of MODIS AOD with $PM_{2.5(PA)}$

Fig. 4 illustrates the correlation between Aqua and Terra AOD_{550nm} and reveals R = 0.942, R^2 = 0.888, and $P < 0.005$. The calibration of two satellite sensors and the retrieval algorithm for MODIS AOD_{550nm} during spatial observations may cause some deviations in the AOD data collected by the two satellites (Green *et al.*, 2009; Gupta *et al.*, 2020; Ichoku *et al.*, 2005; Koelemeijer *et al.*, 2006). However, a significant high correlation indicates that AOD_{550nm} by two satellite measurements can represent reliable and comparable aerosol optical depth, and it can be used for daily averages and combined to compare with other concurrently observed aerosol concentrations such as $PM_{2.5(PA)}$.

Fig. 5 presents a comparison of the hourly average of $PM_{2.5(PA)}$ with the AOD data observed by two satellites at 550 nm wavelength, $AOD_{550nm,}$ without relative humidity correction factor. Fig. 5 also shows the standard deviation and linear best fit line. The best fit line provides an equation, $AOD_{550nm} = 0.038(\pm 0.037) + (0.0068 \pm 0.0006)\ PM_{2.5\ (PA),}$ and the correlation coefficient (R = 0.638, R^2 = 0.407) and *P*-values ($<<$ 0.005) are also obtained from the plot. Based on the correlation between these two parameters, Fig. 5 indicates that surface air pollution, $PM_{2.5(PA),}$ significantly influences aerosol optical depth (AOD_{550nm}).

According to Table 1, the correlation coefficients between AOD_{550nm} and corresponding $PM_{2.5(PA)}$ are improved by dividing AOD_{550nm} by f(RH). In seasons of low temperature, f(RH) has a greater effect on the R^2 than in seasons of higher temperatures. As a result of the temperature inversion at low temperatures, particle concentrations can remain close to the surface due to the significant effect of vertical column AOD correction with f(RH). In low-temperature months, aerosol particles will distribute uniformly near the surface. In summer, however, very few AOD_{550nm} coincide with the corresponding hourly averaged $PM_{2.5(PA)}$ due to persistent monsoon clouds. Correlation results obtained in summer are also given in the table which, however, are less reliable owing to a smaller number of data points on account of monsoon clouds.

Based on the variations in correlation coefficients, meteorological parameters such as relative humidity should be considered when retrieving aerosol optical depths from satellite data (Zhang *et al.*, 2009).

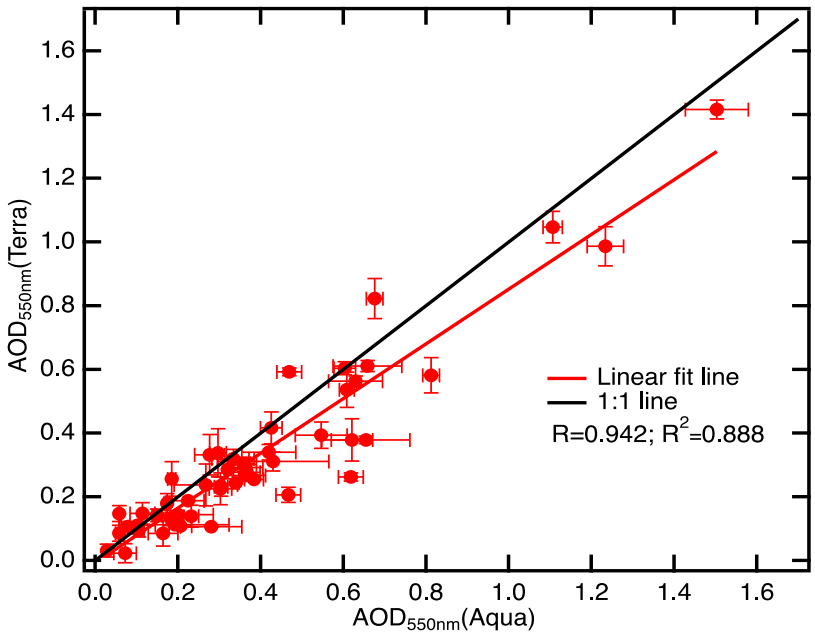

Fig. 4. Scatter plot of MODIS AOD_{550nm} (Terra) vs. MODIS AOD_{550nm} (Aqua) comparing the same day data observed from two satellites in the morning and afternoon.

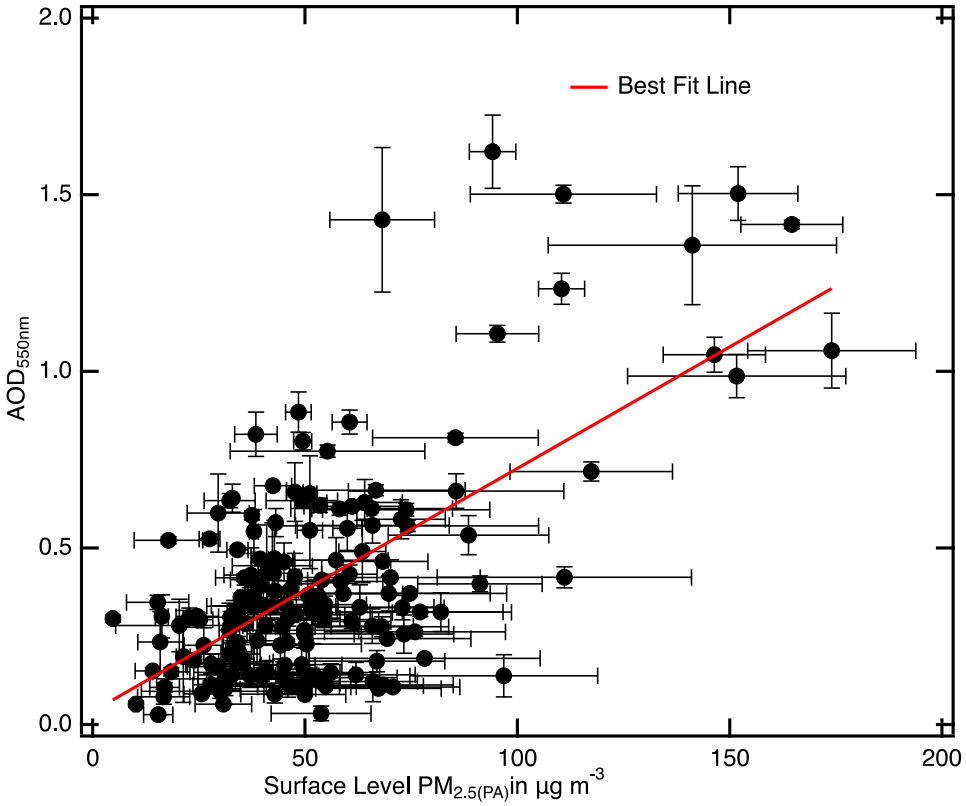

Fig. 5. A comparison between Aqua and Terra Satellites' spatially averaged AOD at 550 nm (AOD_{550nm}) and PurpleAir Monitor's hourly average $PM_{2.5(PA)}$ around the satellite overpass.

Table 1. The correlation coefficients for each seasons using the available one-year 2020 data without and with the f(RH) corrected AOD data vs. $PM_{2.5(PA)}$.

Seasons/Combined	AOD_{550nm} vs. $PM_{2.5(PA)}$	$AOD_{550nm}/f(RH)$ vs. $PM_{2.5(PA)}$
All Data (172)	$R = 0.638$; $R^2 = 0.407$	$R = 0.703$; $R^2 = 0.495$
Winter (Dec–Feb) (28)	$R = 0.643$; $R^2 = 0.413$	$R = 0.780$; $R^2 = 0.608$
Spring (March–May) (77)	$R = 0.653$; $R^2 = 0.426$	$R = 0.713$; $R^2 = 0.508$
Summer (June–Sep) (9)	$R = 0.134$; $R^2 = 0.018$	$R = 0.170$; $R^2 = 0.028$
Autumn (Oct–Nov) (58)	$R = 0.288$; $R^2 = 0.083$	$R = 0.542$; $R^2 = 0.293$

3.3 Seasonal Cluster Analysis

Fig. 6 and supplementary figures Fig. S1 and Fig. S2 show the seasonal clusters of five-day back trajectories over Kathmandu Valley during four seasons at 500 meters, 1000 meters and 1500 meters.

According to percentage contributions, three predominant air masses reach over the Kathmandu valley every season, with five clusters exhibiting the best representation. The cluster analysis shows that fast-moving air masses contribute less, ranging from 1 to 7 percent, to air pollution at the observation site.

At 500 meters, 44% of the winter air mass comes from the Indo-Gangetic plain (IGP), Nepal's south, 38% from the southwest, 16% from the west, and 2% from the west (Fig. 6). The IGP is densely populated, and its aerosol loading is high due to industrial and urban pollution, dust, biomass burning, and the flat land of southern Nepal that lines its northern edge (Regmi *et al.*, 2020). Fig. 6 illustrates the dominance of southerly and southwesterly air masses in winter (December–February) and spring (March–May). The trajectory also indicates that south-easterly air masses from the Bay of Bengal contribute significantly and prominently in summer (June–August), whereas southerly air masses dominate in autumn (September–November). According

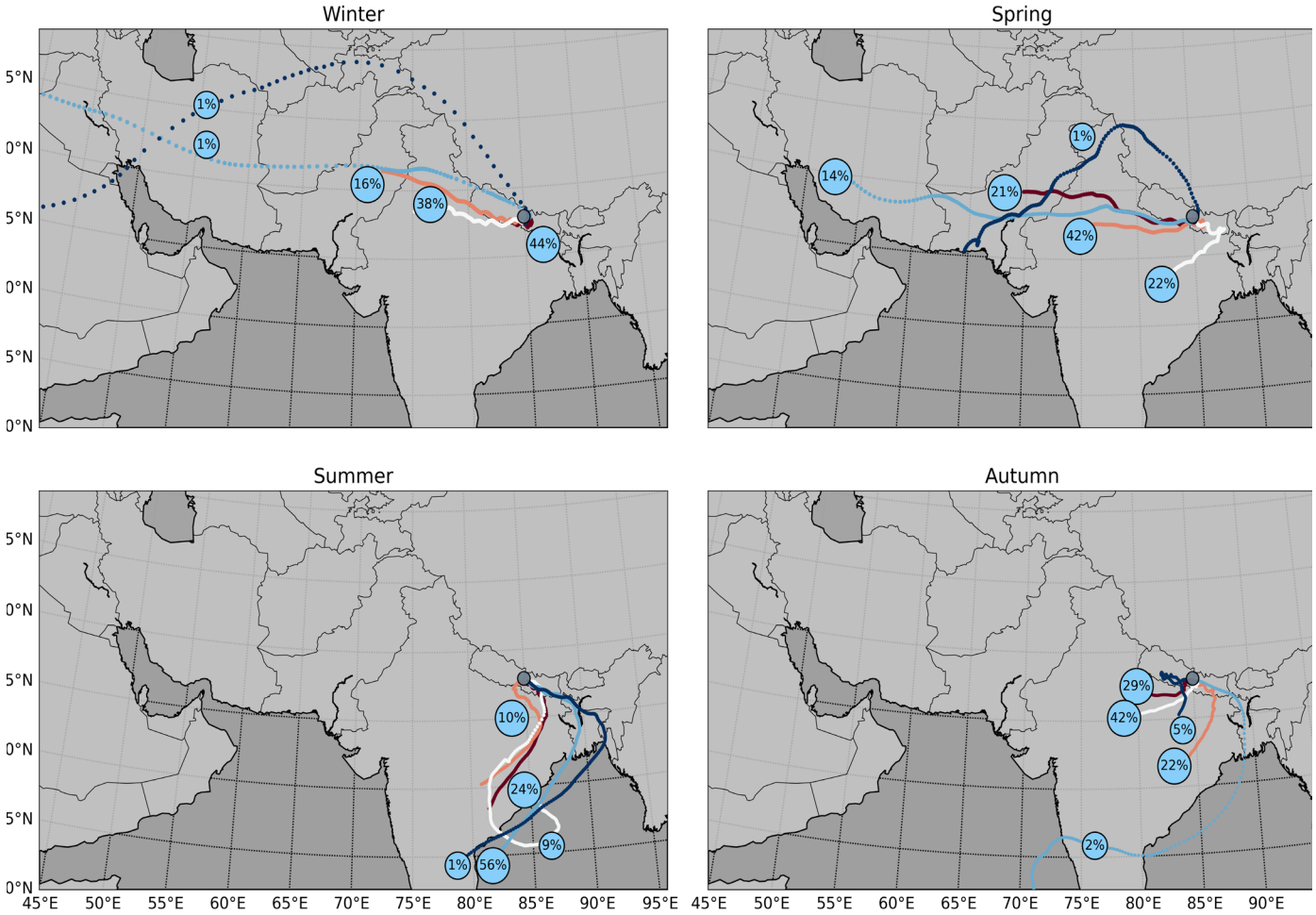

Fig. 6. An analysis of five-day air mass back trajectories computed with Analysis NOAA HYSPLITT and HYSPLIT model reaching Kathmandu at 500 m at different seasons. For each season's cluster analysis, the percentage contribution is presented.

to supplementary figures, Fig. S1 and Fig. S2, the dominant clusters at 1000 meters and 1500 meters are not significantly different from those at 500 meters. Therefore, the air pollution at the observation site is transported vertically from a similar direction to that of 500 meters. At different altitudes, the air mass trajectory crosses the IGP region on its way to the observation site, Kathmandu Valley. As a result, air pollution over the IGP region mainly impacts the aerosol optical depth and the overall vertical air pollution concentration.

4 CONCLUSIONS

The PurpleAir sensor was installed in the Kathmandu Valley, a Himalayan foothill, to determine its capability to measure surface-level small-size particles whose aerodynamic diameter is equal to or smaller than 2.5 micrometers ($PM_{2.5}$). The observation shows that the bimodal particulate concentrations ($PM_{2.5}$) peak at about 8 am and 7 pm, coincident with the density of traffic and other anthropogenic pollutants events, such as cooking and heating, which indicates Kathmandu has significant local sources of outdoor air pollution. In winter, temperature inversion causes particles to remain close to the surface rather than disperse vertically, showing the highest concentrations. During the summer, which is monsoon season, $PM_{2.5}$ levels are low and bimodal variations are smaller. PurpleAir's surface-level $PM_{2.5}$ and MODIS's AOD measurements correlate better with the relative humidity correction factor. For further analyzing the comparison between $PM_{2.5}$ and AOD, boundary layer height (BLH) data can be used, but these data are not available for this study. An air mass cluster analysis shows that transboundary air pollution over different

altitudes at Kathmandu valley is received from different directions and source regions. The contribution of directional airmass varies with the season. The Indo-Gangetic Plain pollutes the atmosphere over Kathmandu during winter, spring, and autumn. In addition to contributing to aerosols over the atmospheric column and, eventually, to column integrated AOD_{550nm}, transboundary air pollution might bias the comparison between $PM_{2.5(PA)}$ and AOD_{550nm}. Moreover, the study establishes that simultaneous measurements of particle concentration at the surface level and AOD over a vertical column allow for the extrapolation of surface-level concentrations using satellite-based AOD, thereby, calling for a more robust and comprehensive analysis of spatial and temporal distribution of $PM_{2.5}$ concentration characteristics and columnar aerosol optical depth.

ACKNOWLEDGMENTS

The authors acknowledge NOAA-ARL and NASA for providing HYSPLIT air mass back trajectories, MODIS satellite air quality data, and Franklin Pierce University for providing the PurpleAir monitor.

DISCLOSURE

Any reference to companies or specific commercial products does not constitute a recommendation, support, or endorsement and we have no conflict of interest to disclose.

SUPPLEMENTARY MATERIAL

Supplementary material for this article can be found in the online version at https://doi.org/10.4209/aaqr.220311

REFERENCES

Adhikari, P., Mejia, J.F. (2022). Impact of transported dust aerosols on precipitation over the Nepal Himalayas using convection-permitting WRF-Chem simulation. Atmos. Environ.: X 15, 100179. https://doi.org/10.1016/j.aeaoa.2022.100179

Altaratz, O., Bar-Or, R.Z., Wollner, U., Koren, I. (2013). Relative humidity and its effect on aerosol optical depth in the vicinity of convective clouds. Environ. Res. Lett. 8, 034025. https://doi.org/10.1088/1748-9326/8/3/034025

Ardon-Dryer, K., Dryer, Y., Williams, J.N., Moghimi, N. (2020). Measurements of $PM_{2.5}$ with PurpleAir under atmospheric conditions. Atmos. Meas. Tech. 13, 5441–5458. https://doi.org/10.5194/amt-13-5441-2020

Aryal, R.K., Lee, B.K., Karki, R., Gurung, A., Baral, B., Byeon, S.H. (2009). Dynamics of $PM_{2.5}$ concentrations in Kathmandu Valley, Nepal. J. Hazard. Mater. 168, 732–738. https://doi.org/10.1016/j.jhazmat.2009.02.086

Aryal, R.P., Voss, K.J., Terman, P.A., Keene, W.C., Moody, J.L., Welton, E.J., Holben, B.N. (2014). Comparison of surface and column measurements of aerosol scattering properties over the western North Atlantic Ocean at Bermuda. Atmos. Chem. Phys. 14, 7617–7629. https://doi.org/10.5194/acp-14-7617-2014

Balasubramanian, S., Domingo, N.G.G., Hunt, N.D., Gittlin, M., Colgan, K.K., Marshall, J.D., Robinson, A.L., Azevedo, I.M.L., Thakrar, S.K., Clark, M.A., Tessum, C.W., Adams, P.J., Pandis, S.N., Hill, J.D. (2021). The food we eat, the air we breathe: A review of the fine particulate matter-induced air quality health impacts of the global food system. Environ. Res. Lett. 16, 103004. https://doi.org/10.1088/1748-9326/ac065f

Baral, B.D., Thapa, K. (2021). Effect of the COVID-19 lockdown on ambient air quality in major cities of Nepal. J. Health Pollut. 11, 210211. https://doi.org/10.5696/2156-9614-11.29.210211

Becker, S., Sapkota, R.P., Pokharel, B., Adhikari, L., Pokhrel, R.P., Khanal, S., Giri, B. (2021). Particulate matter variability in Kathmandu based on in-situ measurements, remote sensing, and reanalysis data. Atmos. Res. 258, 105623. https://doi.org/10.1016/j.atmosres.2021.105623

Brock, C.A., Wagner, N.L., Anderson, B.E., Attwood, A.R., Beyersdorf, A., Campuzano-Jost, P.,

Carlton, A.G., Day, D.A., Diskin, G.S., Gordon, T.D., Jimenez, J.L., Lack, D.A., Liao, J., Markovic, M.Z., Middlebrook, A.M., Ng, N.L., Perring, A.E., Richardson, M.S., Schwarz, J.P., Washenfelder, R.A., *et al.* (2016). Aerosol optical properties in the southeastern United States in summer – Part 1: Hygroscopic growth. Atmos. Chem. Phys. 16, 4987–5007. https://doi.org/10.5194/acp-16-4987-2016

Brock, C.A., Froyd, K.D., Dollner, M., Williamson, C.J., Schill, G., Murphy, D.M., Wagner, N.J., Kupc, A., Jimenez, J.L., Campuzano-Jost, P., Nault, B.A., Schroder, J.C., Day, D.A., Price, D.J., Weinzierl, B., Schwarz, J.P., Katich, J.M., Wang, S., Zeng, L., Weber, R., *et al.* (2021). Ambient aerosol properties in the remote atmosphere from global-scale in situ measurements. Atmos. Chem. Phys. 21, 15023–15063. https://doi.org/10.5194/acp-21-15023-2021

Bui, T.H., Nguyen, D.L., Nguyen, H.H. (2022). Study of aerosol optical properties at two urban areas in the north of Vietnam with the implication for biomass burning impacts. Environ. Sci. Pollut. Res. 29, 41923–41940. https://doi.org/10.1007/s11356-021-15608-5

Calvello, M., Esposito, F., Leone, L., Pavese, G., Restieri, R. (2008). High resolution measurement of aerosol equivalent scale heigth over wide range. 16, 443–448.

Chen, P., Li, C., Kang, S., Yan, F., Zhang, Q., Ji, Z., Tripathee, L., Rupakheti, D., Rupakheti, M., Qu, B., Sillanpää, M. (2016). Source apportionment of particle-bound polycyclic aromatic hydrocarbons in Lumbini, Nepal by using the positive matrix factorization receptor model. Atmos. Res. 182, 46–53. https://doi.org/10.1016/j.atmosres.2016.07.011

Das, M., Das, A., Sarkar, R., Mandal, P., Saha, S., Ghosh, S. (2021). Exploring short term spatio-temporal pattern of $PM_{2.5}$ and PM_{10} and their relationship with meteorological parameters during COVID-19 in Delhi. Urban Clim. 39, 100944. https://doi.org/10.1016/j.uclim.2021.100944

Devi, N.L., Kumar, A., Yadav, I.C. (2020). PM_{10} and $PM_{2.5}$ in Indo-Gangetic Plain (IGP) of India: Chemical characterization, source analysis, and transport pathways. Urban Clim. 33, 100663. https://doi.org/10.1016/j.uclim.2020.100663

Di, Q., Wang, Y., Zanobetti, A., Wang, Y., Koutrakis, P., Choirat, C., Dominici, F., Schwartz, J.D. (2017). Air Pollution and Mortality in the Medicare Population. N. Engl. J. Med. 376, 2513–2522. https://doi.org/10.1056/nejmoa1702747

Duan, J., Huang, R.J., Li, Y., Chen, Q., Zheng, Y., Chen, Y., Lin, C., Ni, H., Wang, M., Ovadnevaite, J., Ceburnis, D., Chen, C., Worsnop, D.R., Hoffmann, T., O'Dowd, C., Cao, J. (2020). Summertime and wintertime atmospheric processes of secondary aerosol in Beijing. Atmos. Chem. Phys. 20, 3793–3807. https://doi.org/10.5194/acp-20-3793-2020

Dusek, U., Frank, G.P., Hildebrandt, L., Curtius, J., Schneider, J., Walter, S., Chand, D., Drewnick, F., Hings, S., Jung, D., Borrmann, S., Andreae, M.O. (2006). Size matters more than chemistry for cloud-nucleating ability of aerosol particles. Science 312, 1375–1378. https://doi.org/10.1126/science.1125261

Edwards, L., Rutter, G., Iverson, L., Wilson, L., Chadha, T.S., Wilkinson, P., Milojevic, A. (2021). Personal exposure monitoring of $PM_{2.5}$ among US diplomats in Kathmandu during the COVID-19 lockdown, March to June 2020. Sci. Total Environ. 772, 144836. https://doi.org/10.1016/j.scitotenv.2020.144836

Green, M., Kondragunta, S., Ciren, P., Xu, C. (2009). Comparison of GOES and MODIS aerosol optical depth (AOD) to aerosol robotic network (AERONET) AOD and IMPROVE $PM_{2.5}$ mass at Bondville, Illinois. J. Air Waste Manage. Assoc. 59, 1082–1091. https://doi.org/10.3155/1047-3289.59.9.1082

Gupta, P., Remer, L.A., Patadia, F., Levy, R.C., Christopher, S. A. (2020). High-resolution gridded level 3 aerosol optical depth data from MODIS. Remote Sens. 12, 2847. https://doi.org/10.3390/rs12172847

Hagan, D.H., Kroll, J.H. (2020). Assessing the accuracy of low-cost optical particle sensors using a physics-based approach. Atmos. Meas. Tech. 13, 6343–6355. https://doi.org/10.5194/amt-13-6343-2020

Haywood, J., Boucher, O. (2000). Estimates of the direct and indirect radiative forcing due to tropospheric aerosols: A review. Rev. Geophys. 38, 513–543. https://doi.org/10.1029/1999RG000078

He, M., Kuerbanjiang, N., Dhaniyala, S. (2020). Performance characteristics of the low-cost Plantower PMS optical sensor. Aerosol Sci. Technol. 54, 232–241. https://doi.org/10.1080/02786826.2019.1696015

Ichoku, C., Remer, L.A., Eck, T.F. (2005). Correction to "Quantitative evaluation and intercomparison of morning and afternoon Moderate Resolution Imaging Spectroradiometer (MODIS) aerosol measurements from Terra and Aqua." J. Geophys. Res. 110, D10S99. https://doi.org/10.1029/2005JD005897

Islam, M.R., Jayarathne, T., Simpson, I.J., Werden, B., Maben, J., Gilbert, A., Praveen, P.S., Adhikari, S., Panday, A.K., Rupakheti, M., Blake, D.R., Yokelson, R.J., DeCarlo, P.F., Keene, W.C., Stone, E.A. (2020). Ambient air quality in the Kathmandu Valley, Nepal, during the pre-monsoon: Concentrations and sources of particulate matter and trace gases. Atmos. Chem. Phys. 20, 2927–2951. https://doi.org/10.5194/acp-20-2927-2020

Jethva, H., Torres, O., Field, R.D., Lyapustin, A., Gautam, R., Kayetha, V. (2019). Connecting crop productivity, residue fires, and air quality over Northern India. Sci. Rep. 9, 16594. https://doi.org/10.1038/s41598-019-52799-x

Jin, X., Li, Z., Wu, T., Wang, Y., Cheng, Y., Su, T., Wei, J., Ren, R., Wu, H., Li, S., Zhang, D., Cribb, M. (2022). The different sensitivities of aerosol optical properties to particle concentration, humidity, and hygroscopicity between the surface level and the upper boundary layer in Guangzhou, China. Sci. Total Environ. 803, 150010. https://doi.org/10.1016/j.scitotenv.2021.150010

Karagulian, F., Belis, C.A., Dora, C.F.C., Prüss-Ustün, A.M., Bonjour, S., Adair-Rohani, H., Amann, M. (2015). Contributions to cities' ambient particulate matter (PM): A systematic review of local source contributions at global level. Atmos. Environ. 120, 475–483. https://doi.org/10.1016/j.atmosenv.2015.08.087

Kasten, F. (1969). Visibility forecast in the phase of pre-condensation. Tellus A 21, 631. https://doi.org/10.3402/tellusa.v21i5.10112

Kitada, T., Regmi, R.P. (2003). Dynamics of air pollution transport in late wintertime over Kathmandu Valley, Nepal: As revealed with numerical simulation. J. Appl. Meteorol. 42, 1770–1798. https://doi.org/10.1175/1520-0450(2003)042<1770:DOAPTI>2.0.CO;2

Koelemeijer, R.B.A., Homan, C.D., Matthijsen, J. (2006). Comparison of spatial and temporal variations of aerosol optical thickness and particulate matter over Europe. Atmos. Environ. 40, 5304–5315. https://doi.org/10.1016/j.atmosenv.2006.04.044

Kotchenruther, R.A., Hobbs, P.V. (1998). Humidification factors of aerosols from biomass burning in Brazil. J. Geophys. Res. 103, 32081–32089. https://doi.org/10.1029/98JD00340

Kotchenruther, R.A. (2020). Recent changes in winter $PM_{2.5}$ contributions from wood smoke, motor vehicles, and other sources in the Northwest U.S. Atmos. Environ. 237, 117724. https://doi.org/10.1016/j.atmosenv.2020.117724

Kumar, N., Chu, A., Foster, A. (2007). An empirical relationship between $PM_{2.5}$ and aerosol optical depth in Delhi Metropolitan. Atmos. Environ. 41, 4492–4503. https://doi.org/10.1016/j.atmosenv.2007.01.046

Kumar, A., Singh, N., Anshumali, Solanki, R. (2018). Evaluation and utilization of MODIS and CALIPSO aerosol retrievals over a complex terrain in Himalaya. Remote Sens. Environ. 206, 139–155. https://doi.org/10.1016/j.rse.2017.12.019

Kumar, P., Goel, A. (2016). Concentration dynamics of coarse and fine particulate matter at and around signalised traffic intersections. Environ. Sci.: Processes Impacts 18, 1220–1235. https://doi.org/10.1039/C6EM00215C

Levy, R.C., Mattoo, S., Munchak, L.A., Remer, L.A., Sayer, A.M., Patadia, F., Hsu, N.C. (2013). The Collection 6 MODIS aerosol products over land and ocean. Atmos. Meas. Tech. 6, 2989–3034. https://doi.org/10.5194/amt-6-2989-2013

Lim, S.S., Vos, T., Flaxman, A.D., Danaei, G., Shibuya, K., Adair-Rohani, H., AlMazroa, M.A., Amann, M., Anderson, H.R., Andrews, K.G., Aryee, M., Atkinson, C., Bacchus, L.J., Bahalim, A.N., Balakrishnan, K., Balmes, J., Barker-Collo, S., Baxter, A., Bell, M.L., Blore, J.D., *et al.* (2012). A comparative risk assessment of burden of disease and injury attributable to 67 risk factors and risk factor clusters in 21 regions, 1990–2010: A systematic analysis for the Global Burden of Disease Study 2010. Lancet 380, 2224–2260. https://doi.org/10.1016/S0140-6736(12)61766-8

Magi, B.I., Cupini, C., Francis, J., Green, M., Hauser, C. (2020). Evaluation of $PM_{2.5}$ measured in an urban setting using a low-cost optical particle counter and a Federal Equivalent Method Beta Attenuation Monitor. Aerosol Sci. Technol. 54, 147–159. https://doi.org/10.1080/02786826.2019.1619915

Mahapatra, P.S., Puppala, S.P., Adhikary, B., Shrestha, K.L., Dawadi, D.P., Paudel, S.P., Panday, A.K. (2019). Air quality trends of the Kathmandu Valley: A satellite, observation and modeling perspective. Atmos. Environ. 201, 334–347. https://doi.org/10.1016/j.atmosenv.2018.12.043

Malm, W.C., Day, D.E., Kreidenweis, S.M. (2000). Light scattering characteristics of aerosols as a function of relative humidity: Part I—A comparison of measured scattering and aerosol concentrations using the theoretical models. J. Air Waste Manage. Assoc. 50, 686–700. https://doi.org/10.1080/10473289.2000.10464117

Mancilla, Y., Herckes, P., Fraser, M.P., Mendoza, A. (2015). Secondary organic aerosol contributions to $PM_{2.5}$ in Monterrey, Mexico: Temporal and seasonal variation. Atmos. Res. 153, 348–359. https://doi.org/10.1016/j.atmosres.2014.09.009

Moody, J.L., Keene, W.C., Cooper, O.R., Voss, K.J., Aryal, R., Eckhardt, S., Holben, B., Maben, J.R., Izaguirre, M.A., Galloway, J.N. (2014). Flow climatology for physicochemical properties of dichotomous aerosol over the western North Atlantic Ocean at Bermuda. Atmos. Chem. Phys. 14, 691–717. https://doi.org/10.5194/acp-14-691-2014

Morawska, L., Thai, P.K., Liu, X., Asumadu-Sakyi, A., Ayoko, G., Bartonova, A., Bedini, A., Chai, F., Christensen, B., Dunbabin, M., Gao, J., Hagler, G.S.W., Jayaratne, R., Kumar, P., Lau, A.K.H., Louie, P.K.K., Mazaheri, M., Ning, Z., Motta, N., Mullins, B., *et al.* (2018). Applications of low-cost sensing technologies for air quality monitoring and exposure assessment: How far have they gone? Environ. Int. 116, 286–299. https://doi.org/10.1016/j.envint.2018.04.018

Mues, A., Lauer, A., Lupascu, A., Rupakheti, M., Kuik, F., Lawrence, M.G. (2018). WRF and WRF-Chem v3.5.1 simulations of meteorology and black carbon concentrations in the Kathmandu Valley. Geosci. Model Dev. 11, 2067–2091. https://doi.org/10.5194/gmd-11-2067-2018

Munir, S., Mayfield, M., Coca, D., Jubb, S.A., Osammor, O. (2019). Analysing the performance of low-cost air quality sensors, their drivers, relative benefits and calibration in cities—A case study in Sheffield. Environ. Monit. Assess. 191, 94. https://doi.org/10.1007/s10661-019-7231-8

Ouimette, J.R., Malm, W.C., Schichtel, B.A., Sheridan, P.J., Andrews, E., Ogren, J.A., Arnott, W.P. (2022). Evaluating the PurpleAir monitor as an aerosol light scattering instrument. Atmos. Meas. Tech. 15, 655–676. https://doi.org/10.5194/amt-15-655-2022

Panday, A.K., Prinn, R.G. (2009). Diurnal cycle of air pollution in the Kathmandu Valley, Nepal: Observations. J. Geophys. Res. 114, D09305. https://doi.org/10.1029/2008JD009777

Pant, P., Harrison, R.M. (2013). Estimation of the contribution of road traffic emissions to particulate matter concentrations from field measurements: A review. Atmos. Environ. 77, 78–97. https://doi.org/10.1016/j.atmosenv.2013.04.028

Pervez, S., Verma, M., Tiwari, S., Chakrabarty, R.K., Watson, J.G., Chow, J.C., Panicker, A.S., Deb, M.K., Siddiqui, M.N., Pervez, Y.F. (2019). Household solid fuel burning emission characterization and activity levels in India. Sci. Total Environ. 654, 493–504. https://doi.org/10.1016/j.scitotenv.2018.11.019

Ramachandran, S., Kedia, S. (2013). Aerosol optical properties over South Asia from ground-based observations and remote sensing: A review. Climate 1, 84–119. https://doi.org/10.3390/cli1030084

Ramanathan, V., Crutzen, P.J., Kiehl, J.T., Rosenfeld, D. (2001). Aerosols, climate, and the hydrological cycle. Science 294, 2119–2124. https://doi.org/10.1126/science.1064034

Regmi, J., Poudyal, K.N., Pokhrel, A., Gyawali, M., Tripathee, L., Panday, A., Barinelli, A., Aryal, R. (2020). Investigation of aerosol climatology and long-range transport of aerosols over Pokhara, Nepal. Atmosphere 11, 874. https://doi.org/10.3390/atmos11080874

Robinson, E.S., Gu, P., Ye, Q., Li, H.Z., Shah, R.U., Apte, J.S., Robinson, A.L., Presto, A.A. (2018). Restaurant impacts on outdoor air quality: Elevated organic aerosol mass from restaurant cooking with neighborhood-scale plume extents. Environ. Sci. Technol. 52, 9285–9294. https://doi.org/10.1021/acs.est.8b02654

Ruzer, L.S., Harley, N.H. (2005). Aerosols handbook: measurement, dosimetry, and health effects. CRC press.

Sarkar, C., Sinha, V., Sinha, B., Panday, A.K., Rupakheti, M., Lawrence, M.G. (2017). Source apportionment of NMVOCs in the Kathmandu Valley during the SusKat-ABC international field campaign using positive matrix factorization. Atmos. Chem. Phys. 17, 8129–8156. https://doi.org/10.5194/acp-17-8129-2017

Sayahi, T., Butterfield, A., Kelly, K.E. (2019). Long-term field evaluation of the Plantower PMS low-

cost particulate matter sensors. Environ. Pollut. 245, 932–940. https://doi.org/10.1016/j.envpol.2018.11.065

Schwartz, J., Dockery, D.W., Neas, L.M. (1996). Is daily mortality associated specifically with fine particles? J. Air Waste Manage. Assoc. 46, 927–939. https://doi.org/10.1080/10473289.1996.10467528

Schwarze, P.E., Øvrevik, J., Låg, M., Refsnes, M., Nafstad, P., Hetland, R.B., Dybing, E. (2006). Particulate matter properties and health effects: Consistency of epidemiological and toxicological studies. Hum. Exp. Toxicol. 25, 559–579. https://doi.org/10.1177/096032706072520

Segura, S., Estellés, V., Utrillas, M.P., Martínez-Lozano, J.A. (2017). Long term analysis of the columnar and surface aerosol relationship at an urban European coastal site. Atmos. Environ. 167, 309–322. https://doi.org/10.1016/j.atmosenv.2017.08.012

Shakya, K.M., Rupakheti, M., Shahi, A., Maskey, R., Pradhan, B., Panday, A., Puppala, S.P., Lawrence, M., Peltier, R.E. (2017). Near-road sampling of $PM_{2.5}$, BC, and fine-particle chemical components in Kathmandu Valley, Nepal. Atmos. Chem. Phys. 17, 6503–6516. https://doi.org/10.5194/acp-17-6503-2017

Shiraiwa, M., Ueda, K., Pozzer, A., Lammel, G., Kampf, C.J., Fushimi, A., Enami, S., Arangio, A.M., Fröhlich-Nowoisky, J., Fujitani, Y., Furuyama, A., Lakey, P.S.J., Lelieveld, J., Lucas, K., Morino, Y., Pöschl, U., Takahama, S., Takami, A., Tong, H., Weber, B., *et al.* (2017). Aerosol health effects from molecular to global scales. Environ. Sci. Technol. 51, 13545–13567. https://doi.org/10.1021/acs.est.7b04417

Shrestha, S., Puppala, S.P., Adhikary, B., Shrestha, K.L., Panday, A.K. (2017). Influence of semi-volatile aerosols on physical and optical properties of aerosols in the Kathmandu Valley. Atmos. Chem. Phys. Discuss. [preprint], https://doi.org/10.5194/acp-2017-287

Stavroulas, I., Grivas, G., Michalopoulos, P., Liakakou, E., Bougiatioti, A., Kalkavouras, P., Fameli, K., Hatzianastassiou, N., Mihalopoulos, N., Gerasopoulos, E. (2020). Field Evaluation of Low-Cost PM Sensors (Purple Air PA-II) Under Variable Urban Air Quality Conditions, in Greece. Atmosphere 11, 926. https://doi.org/10.3390/atmos11090926

van de Hulst, H.C. (1981). Light Scattering by Small Particles (1981st ed.). Dover Publications, Inc.

van Donkelaar, A., Martin, R.V., Brauer, M., Boys, B.L. (2015). Use of satellite observations for long-term exposure assessment of global concentrations of fine particulate matter. Environ. Health Perspect. 123, 135–143. https://doi.org/10.1289/ehp.1408646

Wang, Y.Q. (2014). MeteoInfo: GIS software for meteorological data visualization and analysis. Meteorol. Appl. 21, 360–368. https://doi.org/10.1002/met.1345

Xu, X., Zhang, C. (2020). Estimation of ground-level $PM_{2.5}$ concentration using MODIS AOD and corrected regression model over Beijing, China. PLoS One, 15, 3–15. https://doi.org/10.1371/journal.pone.0240430

Yong, Z. (2016). Plantower PMS5003 Data Manual. 3. http://www.aqmd.gov/docs/default-source/aq-spec/resources-page/plantower-pms5003-manual_v2-3.pdf

Zhang, H., Hoff, R.M., Engel-Cox, J.A. (2009). The relation between moderate resolution imaging spectroradiometer (MODIS) aerosol optical depth and $PM_{2.5}$ over the United States: A geographical comparison by U.S. Environmental Protection Agency regions. J. Air Waste Manage. Assoc. 59, 1358–1369. https://doi.org/10.3155/1047-3289.59.11.1358

Zheng, C., Zhao, C., Zhu, Y., Wang, Y., Shi, X., Wu, X., Chen, T., Wu, F., Qiu, Y. (2017). Analysis of influential factors for the relationship between $PM_{2.5}$ and AOD in Beijing. Atmos. Chem. Phys. 17, 13473–13489. https://doi.org/10.5194/acp-17-13473-2017

Zhong, S., Qian, Y., Zhao, C., Leung, R., Yang, X.Q. (2015). A case study of urbanization impact on summer precipitation in the Greater Beijing Metropolitan Area: Urban heat island versus aerosol effects. J. Geophys. Res. 120, 10903–10914. https://doi.org/10.1002/2015JD023753